Letter

Origin of incommensurate magnetic order in the *R*AlSi magnetic Weyl semimetals (*R* = Pr, Nd, Sm)

Juba Bouaziz,[1,*] Gustav Bihlmayer,[1] Christopher E. Patrick,[2] Julie B. Staunton,[3] and Stefan Blügel[1]

[1]*Peter Grünberg Institut and Institute for Advanced Simulation, Forschungszentrum Jülich & JARA, D-52425 Jülich, Germany*

[2]*Department of Materials, University of Oxford, Parks Road, Oxford OX1 3PH, United Kingdom*

[3]*Department of Physics, University of Warwick, Coventry CV4 7AL, United Kingdom*

(Received 13 November 2023; accepted 19 April 2024; published 8 May 2024)

We investigate rare-earth magnetic Weyl semimetals through first-principles simulations, analyzing the connection between incommensurate magnetic order and the presence of Weyl nodes in the electronic band structure. Focusing on PrAlSi, NdAlSi, and SmAlSi, we demonstrate that the reported helical ordering does not originate from the nesting of topological features at the Fermi surface or the Dzyaloshinskii-Moriya interaction. Instead, the helical order arises from frustrated isotropic short-range superexchange between the 4*f* moments facilitated by *pd* hybridization with the main group elements. Employing a spin Hamiltonian with isotropic exchange and single-ion anisotropy we replicate the experimentally observed helical modulation.

DOI: 10.1103/PhysRevB.109.L201108

Magnetic Weyl semimetals form an exciting class of topological materials [1], owing to the possibility they offer of combining nontrivial topology in both reciprocal momentum space and the space of magnetic order parameters. This raises the prospect of identifying new topological invariants which characterize novel and intriguing physical response properties. In momentum space, Weyl nodes emerge as topologically nontrivial points of contact or crossings between two Kramers' degeneracy-lifted bands, acting as sinks and sources of diverging Berry curvature [2,3]. These correspond to magnetic monopoles strongly affecting electronic response and transport properties, such as anomalous Hall [4] or Nernst effects, magnetoresistance [5,6], or optical properties [7], if they are in the vicinity of the Fermi surface (FS). These emergent Weyl fermions are either a consequence of time-reversal symmetry or spatial-inversion symmetry breaking (ISB) in the presence of the spin-orbit interaction (SOI) [8].

Weyl materials are of great interest magnetically owing to the complex magnetic textures such as spin spirals they can exhibit which can be turned into topological nontrivial textures such as skyrmions with the application of external magnetic fields. ISB, SOI, and magnetism are also the necessary ingredients for chiral Dzyaloshinskii-Moriya magnetic interactions (DMI) [9,10]. DMI can compete with exchange interactions, giving rise to chiral spin-spiral ground states [11] and chiral magnetic skyrmions [12] when magnetic fields are applied. This hints at a relation between the Weyl points and skyrmion formation.

All the more surprising is the recent observation of spiral magnetism in magnetic rare-earth (*R*) *R*AlSi Weyl semimetals and an apparent link to nesting between topologically nontrivial Fermi surface pockets [13–18]. This suggests that the Weyl points are directly related to the much stronger exchange interaction, rather than the weaker DMI, and are the determinants for the magnetic phases. A correlation between band structure topology, i.e., the Weyl points, and the emergence of an incommensurate magnetic order has been found for NdAlSi [13]. The observed helical magnetic order is characterized by a wave vector $\boldsymbol{q}$ that matches the vector connecting the topological features observed in the FS. The incommensurate order in NdAlSi transforms to a commensurate ferrimagnetic one [13] at low temperatures, attributed to the magnetic anisotropy originating from crystal field effects [19]. For SmAlSi [14] helical magnetic order has been identified to persist to lower temperatures and include a topological Hall effect characteristic of the *A* phase [20] in skyrmion materials. PrAlSi exhibits both ferromagnetic and also possibly spin glass or ferromagnetic cluster glass behavior [15]. Thus *R*AlSi compounds have garnered significant interest to be ideal systems for the exploration of the interplay between nontrivial valence band structures and chiral magnetic textures.

The relation between the FS nesting vectors and the helical incommensurate order is suggestive; this assumption is valid in the presence of an indirect exchange or Ruderman-Kittel-Kasuya-Yosida (RKKY) interactions [21–23]. In general, several exchange mechanisms are present in complex magnetic materials, including superexchange (SX) [24,25] and double exchange [26]. A quantitative evidence including all the aforementioned exchange mechanisms which shows a correlation between the topological features at the FS and the magnetic order in the *R*AlSi family is still missing.

In this Letter, for three specific rare-earth semimetallic candidates, PrAlSi, NdAlSi, and SmAlSi, we explore to what extent the RKKY interactions and the topology of the threadbare FSs can contribute to the materials' magnetic orders. Moreover, we also assess whether short-ranged but frustrated SX interactions are preeminent owing to the presence of a quasiband gap. To this end, we examine the magnetic interactions between the rare-earth atoms employing a first-principles approach, which is unbiased as to the exchange mechanism.

*j.bouaziz@fz-juelich.de

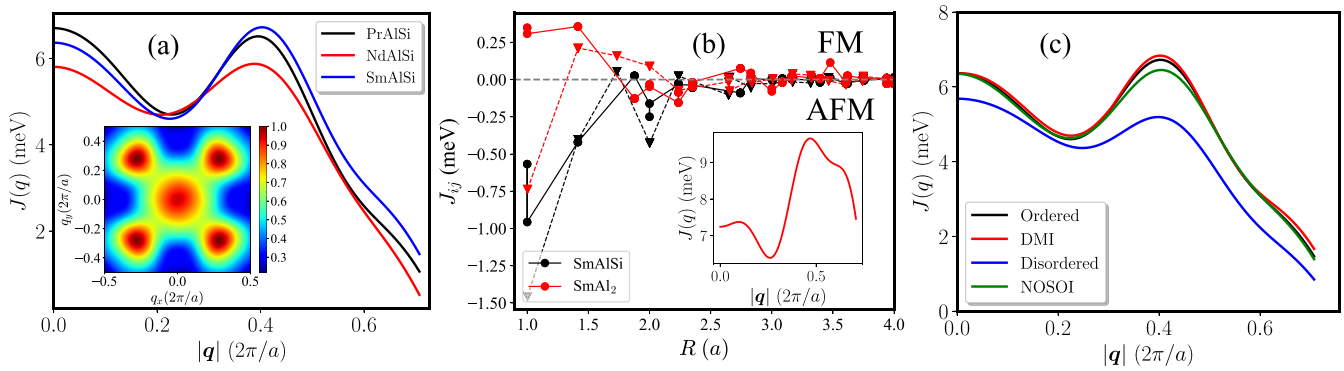

FIG. 1. (a) Maximal eigenvalues $J(\boldsymbol{q})$, indicating a competition between ferromagnetic ($q = 0$) and helical order at q_p in [110] direction, for PrAlSi, NdAlSi, and SmAlSi. The inset highlights the fourfold degenerate peak for SmAlSi. (b) Real-space isotropic exchange interactions in SmAlSi and $SmAl_2$ between $4f$ atoms at distance R, showing different regimes of SX and RKKY. The full (dotted) lines represent intralayer (interlayer) interactions; the inset depicts the $J(\boldsymbol{q})$ for $SmAl_2$. (c) A comparison of $J(\boldsymbol{q})$ for different approximations: SmAlSi compound with ordered Si and Al atoms (black), including the DMI (red), without SOI (green), and with a disordered Si and Al distribution, restoring centrosymmetry, with SOI (blue).

In order to extract some generic insights about the magnetic interactions prevalent in these $4f$ magnetic Weyl semimetal materials, we study a GdAlSi prototype (see Supplemental Material [27]) whose lattice parameters are set to match each *R*AlSi material [21,22]. This enables us to discriminate between RKKY-like magnetic interaction mechanisms, reliant on electronic structure near the Fermi energy in metals, or SX-like mechanisms inherent in magnetic insulators. We find generic competing ferromagnetic and incommensurate helical order interactions. We then perform *ab initio* crystal field theory calculations of single-ion anisotropies [28] to determine the specific magnetic ordered structures.

We employ Hubbard U-corrected density functional theory (DFT+U) [29] calculations to investigate the magnetic interactions and electronic band structures. The calculations are performed with the all-electron full-potential Korringa-Kohn-Rostoker (KKR) Green's function method [30], including scalar relativistic effects and spin-orbit coupling self-consistently [31]. We compute the magnetic interactions between the $4f$ magnetic atoms using the infinitesimal rotation method [32–34]. The real space exchange interactions tensor and the corresponding lattice Fourier transforms are carefully inspected, unveiling the different exchange mechanisms at play. The lattice constants employed in the calculations are taken from experiment (Supplemental Material [27]).

A minimal spin Hamiltonian, $\mathcal{H}_{\rm m}$, for a noncentrosymmetric crystal, with the magnetic interactions, which we have calculated *ab initio*, is given by

$$\mathcal{H}_{\rm m} = -\frac{1}{2}\sum_{i\neq j} J_{ij}\,\boldsymbol{m}_i\cdot\boldsymbol{m}_j + \frac{1}{2}\sum_{i\neq j}\boldsymbol{D}_{ij}\cdot(\boldsymbol{m}_i\times\boldsymbol{m}_j) - \sum_i K_i\,(\boldsymbol{e}_n\cdot\boldsymbol{m}_i)^2. \quad (1)$$

$\boldsymbol{m}_i$ is the direction of the magnetic moment at an R site i and $\boldsymbol{e}_n$ is the direction of the (effective) easy axis specified with respect to the crystal structure. The first term refers to the isotropic Heisenberg interactions, the second the antisymmetric Dzyaloshinskii–Moriya interactions (DMI) [9,10], which promote chiral spin textures [35], and the third the crystal field single-ion anisotropy at the rare-earth sites (K_i). We can safely neglect the two-ion anisotropy due to its small size compared to K_i. In order to find the origin of the helical order observed in the *R*AlSi family, we inspect the Fourier transform $\mathcal{J}^{\alpha\beta}_{mn}(\boldsymbol{q})$ of the magnetic exchange interactions. m and n denote the atomic indices in the unit cell labeling the two magnetic atoms in *R*AlSi; α and β indicate the $\{x, y, z\}$ components. The maximal eigenvalue $J(\boldsymbol{q})$ of the Fourier transform matrix $\mathcal{J}^{\alpha\beta}_{mn}(\boldsymbol{q})$ provides information on the magnetic order and an estimate of the transition temperature $T_{\rm N}$. $J(\boldsymbol{q})$ is depicted in Fig. 1(a) for our Gd prototype with the lattice structures of PrAlSi, NdAlSi, and SmAlSi, respectively (Supplemental Material [27]). In each case, we see two peaks of roughly comparable magnitude at $\boldsymbol{q} = 0$, indicative of intralayer ferromagnetic correlations, and at $\boldsymbol{q} = \frac{2\pi}{a}(q, q, 0)$ with $q \approx 0.3$ (a being the in-plane lattice constant), which describes single-q spiroidal magnetic correlations [22,23]. The dominant peak determines the magnetic order that will form below the transition temperature. For PrAlSi, the maximum peak occurs at $\boldsymbol{q}_p = (0, 0, 0)$ and the ferromagnetic order within each layer is favored as observed experimentally in Ref. [15], while, for the NdAlSi case, the maximum peak occurs at $\boldsymbol{q}_p = \frac{2\pi}{a}(q_p, q_p, 0)$ with $q_p = 0.273$ in agreement with the experimental value of $q_p^{\rm expt} = \frac{1}{3} + \delta$ [13]. However, the small energy difference $\Delta E = 0.07$ meV between the spiral and ferromagnetic states, $J(\boldsymbol{q}_p) - J(\boldsymbol{0})$, is not sufficient to overcome the magnetic anisotropy energy caused by the crystal field, suppressing the helical ordering at low temperature and enforcing a ferromagnetic order intralayer [13]. For the case of SmAlSi, the maximum peak occurs once more at a finite q with $\boldsymbol{q}_p = \frac{2\pi}{a}(q_p, q_p, 0)$ and $q_p = 0.283$, very close to the experimental value $q_p^{\rm expt} = 0.33$ [14]. Compared to the NdAlSi case, the energy difference here is much larger, $\Delta E = 0.36$ meV, and together with the reduction of the

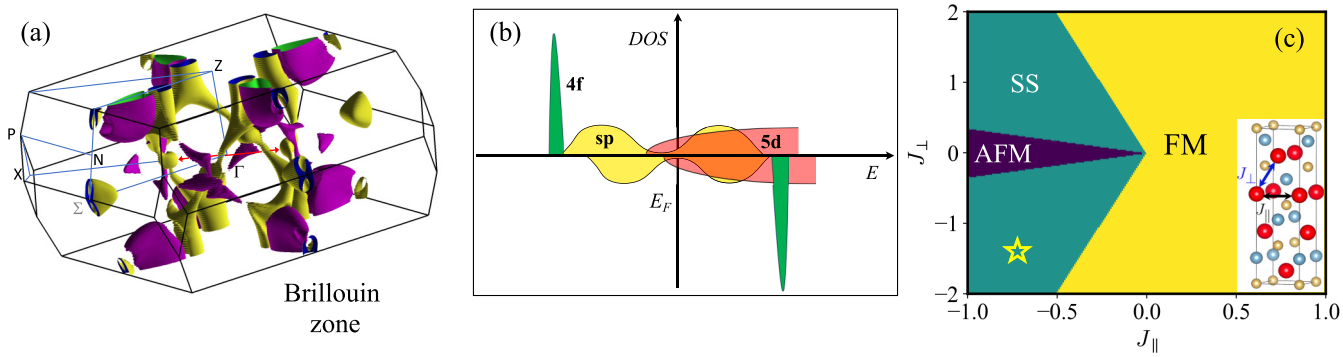

FIG. 2. (a) Complex FS of semimetallic SmAlSi, with the high-symmetry points and Brillouin zone indicated. The red arrow indicates the nontrivial nesting vector at the FS discussed in Ref. [14]. (b) Schematic representation of the low semimetallic density of states (DOS) at E_F displaying the sp band and the hybridization with spin-polarized d electrons. (c) A simplified two-parameter phase diagram incorporating nearest neighbor intralayer ($J_\parallel$) and interlayer ($J_\perp$) interactions [see inset in Fig. 2(c)], illustrating the emergence of spin-spiral (SS) order within each rare-earth layer under antiferromagnetic ($J_\parallel < 0$) intralayer exchange interactions. Phases with (anti)ferromagnetic order within each layer are labeled with FM (AFM). The yellow star indicates the value of the nearest neighbors' exchange interactions calculated *ab initio*.

crystal field effects owing to the lanthanide lattice contraction of heavier $4f$ elements (see discussion below), this results in a persisting incommensurate order at low temperatures [14]. At these temperatures quantum effects play a role in determining the transition temperatures. Nonetheless, estimating T_N using a mean-field, classical spin prescription, $T_N = J(\boldsymbol{q}_p)/3k_B$, with k_B being the Boltzmann constant, we find $T_N \simeq 25$ K, which is of the same order of magnitude as the experimentally measured T_N [14].

To determine the dominant exchange contribution in *R*AlSi, we examine Fig. 1(b), where the black curves represent the isotropic exchange interactions J_{ij} as functions of interatomic distance. The full (dotted) line represents short-range, antiferromagnetic intralayer (interlayer) interactions indicating a SX mechanism [24] over a weak RKKY exchange. Despite the coexistence with RKKY-like interactions, the scarcity of electronic states near E_F and the threadbare FS [Fig. 2(a)] favor the dominance of SX interactions.

Figure 2(a) displays the FS of the Gd prototype (with the SmAlSi lattice constant) obtained using the FLEUR code [36] (see Supplemental Material [27]). The FS occupies only a small portion of the Brillouin zone owing to the low density of states near the Fermi energy (E_F), i.e., the semimetallic nature of SmAlSi. The suggested nesting between the nontrivial Fermi pockets is indicated by a red arrow in Fig. 2(a). However, the FS sheets are not parallel and exhibit a three-dimensional dispersion, which does not fulfill the nesting condition required to stabilize incommensurate ordering. This observation aligns with recent findings in Ref. [37], where the computation of the Lindhard susceptibility, based on the FS, does not indicate a finite-q helical ordering.

To further elaborate on this balance between RKKY and SX interactions, we analyze a related but metallic compound $GdAl_2$ with the same lattice constants (SmAlSi). Substituting Si with Al removes one electron from the system, shifting E_F below the semimetallic gap (see Supplemental Material [27]). The resulting magnetic interactions are shown in Fig. 1(b). In contrast to GdAlSi, they exhibit an oscillatory long-range behavior, indicating that the RKKY interactions dominate over SX in this metallic regime, favoring a spiroidal state [see inset of Fig. 1(b)]. The SX mechanism in *R*AlSi compounds can be understood through an analysis of the density of states, as depicted schematically in Fig. 2(b). In these compounds, the $4f$ electrons induce a local Zeeman magnetic field, causing spin polarization of the rare-earth's $5d$ electrons. These induced $5d$ magnetic moments interact with the p electrons at different sites through the nonmagnetic Si and Al atoms. The SX interactions can be described in terms of a charge-transfer model similar to the transition-metal oxides one [38]: $J_{ij} \propto -t_{pd}^4/\Delta^3$, where t_{pd} represents the hopping integral between the d and p orbitals and Δ is the charge-transfer energy. A comparable scenario arises in Gd monopnictides where SX competes with RKKY interactions [39]. Lastly, while maintaining the same crystalline configuration but substituting Gd with Eu (EuAlSi), the R valence $5d$ electrons are removed (the rare earth atoms are divalent rather than trivalent), leaving only sp electrons that scatter off the localized $4f$ electrons. This ultimately leads to an RKKY interaction among the $4f$ moments (Supplemental Material [27]), once again emphasizing the significant role of $5d$ electrons in generating the SX mechanism.

Although our analysis thus far indicates a dominant role for SX, we now investigate the interplay between the Weyl points and the incommensurate helical ordering by considering two distinct cases: first excluding SOI, where the band structure contains nodal lines [37,40], and second including SOI which introduces gaps in the nodal lines and generates Weyl points at specific symmetry dictated positions in k space [40]. Figure 1(c) depicts $J(q)$ of SmAlSi for these two cases—including (black curve) and excluding the SOI (green curve). While $J(\boldsymbol{q})$ differs slightly near $(q_p, q_p, 0)$, the finite-q peak structure remains and incommensurate order is still favored over ferromagnetism with an energy barrier $\Delta E = 0.10$ meV. This demonstrates that a stable helical order can form in the absence of Weyl points. Moreover, despite the presence of Weyl nodes in the electronic band structure of PrAlSi, $J(\boldsymbol{q})$ has the maximal value at $\boldsymbol{q} = (0, 0, 0)$ favoring a collinear order even without the inclusion of single-ion anisotropy [see Fig. 1(a)].

We now inspect the role of inversion-symmetry breaking on the magnetic order of SmAlSi. The centrosymmetry

can be restored using a 50%-50% alloy of Al and Si species at each site, i.e., $Sm(Al_{0.5}Si_{0.5})_2$. This is achieved computationally using the coherent potential approximation [41]. The electronic band structure obtained for this centrosymmetric SmAlSi alloy is given in the Supplemental Material [27]. Centrosymmetry leads to the removal of the Weyl points (note that the DMI is suppressed as well) and the disorder smears out the electronic bands near the Fermi energy [42]. The resulting $J(\boldsymbol{q})$, shown in Fig. 1(c) (blue curve), supports ferromagnetic order prevailing in the alloy ($\Delta E = -0.17$ meV), but the finite-q peak persists indicating that the helical order does not originate from inversion symmetry breaking or the Weyl points. Lastly, inclusion of DMI (red curve) is found to have a minimal effect owing to its weak magnitude—while it breaks the $\pm q$ reciprocity reducing the fourfold degeneracy [inset Fig. 1(a)], it does not alter the position or the magnitude of the finite-q peak in $J(\boldsymbol{q})$ which is purely driven by isotropic exchange.

The crystal field effects play an important role in the *R*AlSi family. The $4f$ electrons' electronic configuration in *R*AlSi has an atomiclike behavior in accordance with Hund's rules [14], which in turn determines the shape of the $4f$ charge cloud. This charge is subjected to the crystal field (CF) originating from the valence electrons and surrounding ions. Considering that the noncollinear order is driven by the isotropic exchange interactions and not crystal fields effects, the tetragonal uniaxial magnetic anisotropy constant K_i is computed from fitting the classical CF energy differences [43] while rotating the $4f$ moment from the c axis to the a axis. The crystal field parameters are obtained within the yttrium analog approach [28] (see Supplemental Material [27]). Both PrAlSi and NdAlSi display an out-of-plane anisotropy, in agreement with the experimental observation [13]: PrAlSi has a high value of $K_i = 2.593$ meV, while the NdAlSi constant is one order of magnitude smaller $K_i = 0.218$ meV. On the other hand, SmAlSi prefers a canted easy anisotropy axis $\boldsymbol{e}_n$ along the $(\theta_n, \phi_n) = (60^\circ, 45^\circ)$ direction with respect to tetragonal basis vectors, with an anisotropy constant of $K_i = 0.13$ meV.

We extract the following minimal atomistic spin model in reciprocal space to understand the formation of a helical order in *R*AlSi from the short-ranged, antiferromagnetic interactions ($J < 0$):

$$J_{\mathrm{nn}}^{\parallel}(\boldsymbol{q}) = 2J_{\parallel}(\cos q_x a + \cos q_y a),$$
$$J_{\mathrm{nn}}^{\perp}(\boldsymbol{q}) = 2J_{\perp}[\cos(q_x a/2) + \cos(q_y a/2)]. \qquad (2)$$

Hereby, we consider an isotropic Heisenberg model with nearest-neighbor intralayer ($J_{\parallel}$) and interlayer ($J_{\perp}$) interactions as depicted in the inset of Fig. 2(c). We construct the phase diagram shown in Fig. 2(c) by varying $J_{\parallel}$ and $J_{\perp}$ and identifying the in-plane $\boldsymbol{q}$ which maximizes the eigenvalue $J(\boldsymbol{q})$. Within each rare-earth layer three phases emerge, namely a ferromagnetic (FM), antiferromagnetic (AFM), and spin spiral (SS) phase. For $J_{\parallel} < 0$, the AFM phase switches to a SS phase as the magnitude of $J_{\perp}$ increases. For SmAlSi, the $J_{\parallel}$ and $J_{\perp}$ parameters lie in the region of the SS phase as can be seen from the first-principles results in Fig. 1(b).

Now, for the case of SmAlSi, considering (short range) magnetic interactions J_{ij} in real space up to $2.5a$, with $K_i = 0.13$ meV, $\boldsymbol{e}_n = (60^\circ, 45^\circ)$, and neglecting the DMI, we minimize the Hamiltonian $\mathcal{H}_{\mathrm{m}}$ (1) by solving the Landau-Lifshitz-Gilbert equation as implemented in the SPIRIT code [44]. The resulting helical order for the first sublattice is depicted in Fig. 3(a) (top view), featuring a propagation vector $\boldsymbol{q} = \frac{2\pi}{a}(q, q, 0)$ with $q = 0.33$ consistent with the maximum of $J(\boldsymbol{q})$ for SmAlSi. Figure 3(b) illustrates the helimagnetic structure where both sublattices show a similar magnetic order but with a positional shift owing to the stacking along the c axis. Besides the helical order, a solution slightly higher in energy ($\Delta E = 0.05$ meV) features moments antiferromagnetically coupled along the c axis, as depicted in Fig. 3(d). The helical order can transform to this antiferromagnetic state under high-field conditions or with thermal fluctuations. To explore the emergence of noncollinear spin textures, we apply a magnetic field along the easy-axis [23] $\boldsymbol{e}_n$. The resulting state is shown in Fig. 3(c). We observe a canting of the moments towards the $+z$ direction, but no skyrmion lattice phases can form owing to the short period of the magnetic structure ($3a$). The helical order remains the most stable one.

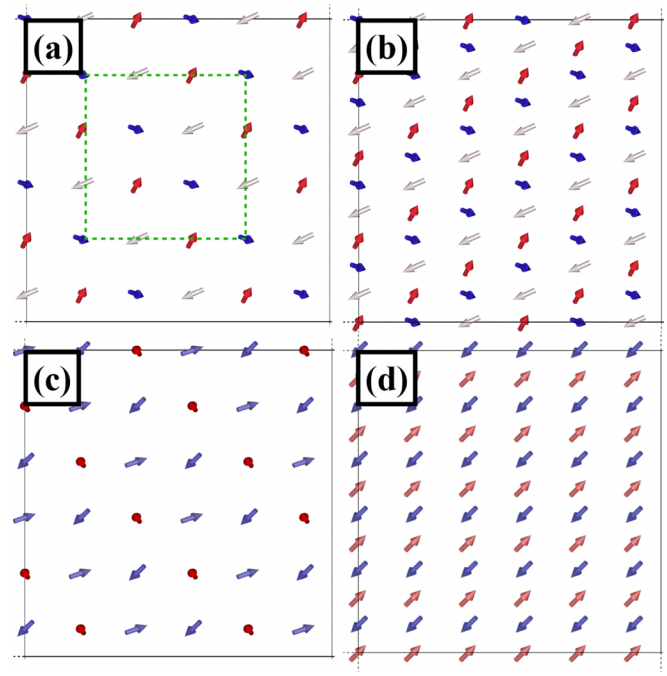

FIG. 3. (a) Helical magnetic structure of SmAlSi in the presence of frustrated isotropic exchange interactions and a canted magnetic anisotropy; the colors indicate the m_z component (blue: $m_z = -1$; red: $m_z = 1$; white: $m_z = 0$). The green dashed square denotes magnetic unit cell. (b) Same as in (a), including sublattice two. (c) Same as in (a) including an external magnetic field ($B = 4$ T) along the easy axis ($60^\circ, 45^\circ$). (d) Stacked antiferromagnetic state along the c axis with higher energy compared to (b).

Coming back to the above mentioned nonconventional contribution to the Hall signal observed experimentally for SmAlSi when a magnetic field is applied [14], we conjecture that this signal can be interpreted in terms of the recently introduced noncollinear Hall effect [45]. This effect emerges from the interference between noncollinear magnetism and spin-orbit interactions in a noncentrosymmetric environment, without invoking the presence of magnetic skyrmions. Likely,

this unconventional Hall signal originates from the scattering of Weyl fermions on the helical magnetic background.

In summary, we have examined three members from the *R*AlSi family, recently proposed as materials where Weyl-mediated RKKY interactions generate helical ordering. Our findings demonstrate that neither the Weyl points nor the RKKY interactions provide the predominant mechanism owing to the presence of a low density of states near the Fermi energy in these semimetals. Instead, we find a significant *p*-*d* antiferromagnetic SX contribution. The competition of these isotropic SX interactions between different atoms leads to a helical order with a short period of approximately three lattice constants, all without the assistance of DMI. Our *ab initio* calculations reveal a strong magnetic anisotropy arising from crystal field effects for PrAlSi and NdAlSi, locking the moments into a collinear configuration. In contrast, the magnetic anisotropy in SmAlSi is much lower, which allows for the formation of a helical incommensurate order at low temperatures. Lastly, the short period of the spin spiral does not permit the emergence of a skyrmion lattice when external magnetic fields are applied.

For future prospects, our *ab initio* computed crystal field coefficients serve as a theoretical input for ongoing experimental investigations using inelastic neutron scattering to understand the complex magnetic structures and crystal field excitations of the RAlSi compounds. Meanwhile, our analysis of the Fermi surface and electronic band structure in different configurations, including chemically ordered, paramagnetic, and chemically disordered, provides very useful insights to interpret experimental photoemission data [37]. Finally, alloying Al and Si with other elements from the same family or applying strain may drive the exchange parameters of the compound closer to the SS-FM phase boundaries of the phase diagram [Fig. 2(b)], leading to longer-period helical orders which may be turned into a skyrmion lattice by applying an external magnetic field. This provides an ideal platform to study the interplay between the topology of the magnetic textures in real space and that of Weyl fermions in reciprocal space.

We thank C. Timm, C. L. Broholm, N. Kiselev, and A. Knoll for fruitful discussions. J.B. and S.B. acknowledges financial support from the European Research Council (ERC) under the European Union's Horizon 2020 research and innovation program (Grant No. 856538, project "3D MAGiC"). S.B. acknowledges financial support from Deutsche Forschungsgemeinschaft (DFG) through CRC 1238, Control and Dynamics of Quantum Materials: Spin orbit coupling, correlations, and topology (Project No. 277146847 C01). J.B.S. acknowledges support from UK EPSRC Grant No. EP/M028941/1. J.B., S.B., and G.B. acknowledge computing time granted by the JARA-CSD and VSR Resource Allocation Board provided on the supercomputers CLAIX at RWTH Aachen University and JURECA at Jülich Supercomputer Centre under Grants No. jara0219 and No. jiff13.

[1] N. Kumar, S. N. Guin, K. Manna, C. Shekhar, and C. Felser, Topological quantum materials from the viewpoint of chemistry, Chem. Rev. **121**, 2780 (2021).

[2] M. Z. Hasan, G. Chang, I. Belopolski, G. Bian, S.-Y. Xu, and J.-X. Yin, Weyl, Dirac and high-fold chiral fermions in topological quantum matter, Nat. Rev. Mater. **6**, 784 (2021).

[3] B. Yan and C. Felser, Topological materials: Weyl semimetals, Annu. Rev. Condens. Matter Phys. **8**, 337 (2017).

[4] D. Destraz, L. Das, S. S. Tsirkin, Y. Xu, T. Neupert, J. Chang, A. Schilling, A. G. Grushin, J. Kohlbrecher, L. Keller *et al.*, Magnetism and anomalous transport in the Weyl semimetal PrAlGe: possible route to axial gauge fields, npj Quantum Mater. **5**, 5 (2020).

[5] X. Huang, L. Zhao, Y. Long, P. Wang, D. Chen, Z. Yang, H. Liang, M. Xue, H. Weng, Z. Fang *et al.*, Observation of the Chiral-anomaly-induced negative magnetoresistance in 3D Weyl semimetal TaAs, Phys. Rev. X **5**, 031023 (2015).

[6] A. Knoll, C. Timm, and T. Meng, Negative longitudinal magnetoconductance at weak fields in Weyl semimetals, Phys. Rev. B **101**, 201402(R) (2020).

[7] N. Nagaosa, T. Morimoto, and Y. Tokura, Transport, magnetic and optical properties of Weyl materials, Nat. Rev. Mater. **5**, 621 (2020).

[8] A. Knoll and C. Timm, Classification of Weyl points and nodal lines based on magnetic point groups for spin-$\frac{1}{2}$ quasiparticles, Phys. Rev. B **105**, 115109 (2022).

[9] I. Dzyaloshinsky, A thermodynamic theory of "weak" ferromagnetism of antiferromagnetics, J. Phys. Chem. Solids **4**, 241 (1958).

[10] T. Moriya, Anisotropic superexchange interaction and weak ferromagnetism, Phys. Rev. **120**, 91 (1960).

[11] I. E. Dzyaloshinskii, Theory of helicoidal structures in antiferromagnets. III, J. Exptl. Theoret. Phys. (U.S.S.R.) **47**, 992 (1964) [Sov. Phys. JETP **20**, 665 (1965)].

[12] A. N. Bogdanov and D. A. Yablonskii, Thermodynamically stable "vortices" in magnetically ordered crystals. The mixed state of magnets, Zh. Eksp. Teor. Fiz. **95**, 178 (1989).

[13] J. Gaudet, H.-Y. Yang, S. Baidya, B. Lu, G. Xu, Y. Zhao, J. A. Rodriguez-Rivera, C. M. Hoffmann, D. E. Graf, D. H. Torchinsky *et al.*, Weyl-mediated helical magnetism in NdAlSi, Nat. Mater. **20**, 1650 (2021).

[14] X. Yao, J. Gaudet, R. Verma, D. E. Graf, H.-Y. Yang, F. Bahrami, R. Zhang, A. A. Aczel, S. Subedi, D. H. Torchinsky, J. Sun, A. Bansil, S.-M. Huang, B. Singh, P. Blaha, P. Nikolić, and F. Tafti, Large topological Hall effect and spiral magnetic order in the Weyl semimetal SmAlSi, Phys. Rev. X **13**, 011035 (2023).

[15] M. Lyu, J. Xiang, Z. Mi, H. Zhao, Z. Wang, E. Liu, G. Chen, Z. Ren, G. Li, and P. Sun, Nonsaturating magnetoresistance, anomalous Hall effect, and magnetic quantum oscillations in the ferromagnetic semimetal PrAlSi, Phys. Rev. B **102**, 085143 (2020).

[16] P. Puphal, V. Pomjakushin, N. Kanazawa, V. Ukleev, D. J. Gawryluk, J. Ma, M. Naamneh, N. C. Plumb, L. Keller, R. Cubitt *et al.*, Topological magnetic phase in the candidate Weyl semimetal CeAlGe, Phys. Rev. Lett. **124**, 017202 (2020).

[17] H.-Y. Yang, B. Singh, J. Gaudet, B. Lu, C.-Y. Huang, W.-C. Chiu, S.-M. Huang, B. Wang, F. Bahrami, B. Xu *et al.*,

Noncollinear ferromagnetic Weyl semimetal with anisotropic anomalous Hall effect, Phys. Rev. B **103**, 115143 (2021).
[18] H.-R. Chang, J. Zhou, S.-X. Wang, W.-Y. Shan, and D. Xiao, RKKY interaction of magnetic impurities in Dirac and Weyl semimetals, Phys. Rev. B **92**, 241103(R) (2015).
[19] J. Jensen and A. R. Mackintosh, *Rare Earth Magnetism: Structures and Excitations* (Clarendon, Oxford, 1991).
[20] A. Neubauer, C. Pfleiderer, B. Binz, A. Rosch, R. Ritz, P. G. Niklowitz, and P. Böni, Topological Hall effect in the *A* phase of MnSi, Phys. Rev. Lett. **102**, 186602 (2009).
[21] I. D. Hughes, M. Däne, A. Ernst, W. Hergert, M. Lüders, J. Poulter, J. B. Staunton, A. Svane, Z. Szotek, and W. M. Temmerman, Lanthanide contraction and magnetism in the heavy rare earth elements, Nature (London) **446**, 650 (2007).
[22] E. Mendive-Tapia and J. B. Staunton, Theory of magnetic ordering in the heavy rare earths: *Ab initio* electronic origin of pair- and four-spin interactions, Phys. Rev. Lett. **118**, 197202 (2017).
[23] J. Bouaziz, E. Mendive-Tapia, S. Blügel, and J. B. Staunton, Fermi-surface origin of skyrmion lattices in centrosymmetric rare-earth intermetallics, Phys. Rev. Lett. **128**, 157206 (2022).
[24] P. W. Anderson, Antiferromagnetism. Theory of superexchange interaction, Phys. Rev. **79**, 350 (1950).
[25] I. V. Solovyev and K. Terakura, Zone boundary softening of the spin-wave dispersion in doped ferromagnetic manganites, Phys. Rev. Lett. **82**, 2959 (1999).
[26] I. V. Solovyev, Optimized effective potential for the extended Hubbard model, Phys. Rev. B **60**, 8550 (1999).
[27] See Supplemental Material at http://link.aps.org/supplemental/10.1103/PhysRevB.109.L201108 for further details on the Gd-prototype approach, the Fourier transform of the magnetic interactions, electronic density of states, electronic band structures of SmAlSi for various cases (chemically ordered, chemically disordered, and paramagnetic state), Fermi surfaces, and derivation of the single ion anisotropy using crystal field theory, which includes Refs. [9,10,14,22,28,29,33,34,36,40,41,43,44,46–62].
[28] C. E. Patrick and J. B. Staunton, Crystal field coefficients for yttrium analogues of rare-earth/transition-metal magnets using density-functional theory in the projector-augmented wave formalism, J. Phys.: Condens. Matter **31**, 305901 (2019).
[29] S. L. Dudarev, P. Liu, D. A. Andersson, C. R. Stanek, T. Ozaki, and C. Franchini, Parametrization of LSDA + U for noncollinear magnetic configurations: Multipolar magnetism in UO_2, Phys. Rev. Mater. **3**, 083802 (2019).
[30] P. Rüssmann, D. Antognini Silva, G. Géranton, D. S. G. Bauer, P. Baumeister, P. F. Bornemann, J. Bouaziz, S. Brinker, J. Chico, P. H. Dederichs, B. H. Drittler, F. Dos Santos, M. dos Santos Dias, N. Essing, I. Klepetsanis, A. Kosma, N. H. Long, S. Lounis, P. Mavropoulos, E. Mendive Tapia *et al.*, JuDFT-team/JuKKR: v3.6, version v3.6, Zenodo (2022).
[31] D. S. G. Bauer, Development of a relativistic full-potential first-principles multiple scattering Green function method applied to complex magnetic textures of nanostructures at surfaces, Forschungszentrum Jülich, 2014, https://publications.rwth-aachen.de/record/229375.
[32] A. I. Liechtenstein, M. I. Katsnelson, and V. A. Gubanov, Exchange interactions and spin-wave stiffness in ferromagnetic metals, J. Phys. F **14**, L125 (1984).
[33] H. Ebert and S. Mankovsky, Anisotropic exchange coupling in diluted magnetic semiconductors: *Ab initio* spin-density functional theory, Phys. Rev. B **79**, 045209 (2009).
[34] I. V. Solovyev, Exchange interactions and magnetic force theorem, Phys. Rev. B **103**, 104428 (2021).
[35] S. Heinze, K. Von Bergmann, M. Menzel, J. Brede, A. Kubetzka, R. Wiesendanger, G. Bihlmayer, and S. Blügel, Spontaneous atomic-scale magnetic skyrmion lattice in two dimensions, Nat. Phys. **7**, 713 (2011).
[36] D. Wortmann, G. Michalicek, N. Baadji, M. Betzinger, G. Bihlmayer, J. Bröder, T. Burnus, J. Enkovaara, F. Freimuth, C. Friedrich, C.-R. Gerhorst, S. Granberg Cauchi, U. Grytsiuk, A. Hanke, J.-P. Hanke, M. Heide, S. Heinze, R. Hilgers, H. Janssen, D. A. Klüppelberg *et al.*, FLEUR, Zenodo (2024).
[37] Y. Zhang, Y. Gao, X.-J. Gao, S. Lei, Z. Ni, J. S. Oh, J. Huang, Z. Yue, M. Zonno, S. Gorovikov *et al.*, Kramers nodal lines and Weyl fermions in SmAlSi, Commun. Phys. **6**, 134 (2023).
[38] V. A. Gubanov, A. I. Liechtenstein, and A. V. Postnikov, *Magnetism and the Electronic Structure of Crystals* (Springer Science & Business Media, New York, 2012), Vol. 98.
[39] C.-G. Duan, R. F. Sabiryanov, W.-N. Mei, P. A. Dowben, S. S. Jaswal, and E. Y. Tsymbal, Magnetic ordering in Gd monopnictides: Indirect exchange versus superexchange interaction, Appl. Phys. Lett. **88**, 182505 (2006).
[40] G. Chang, B. Singh, S.-Y. Xu, G. Bian, S.-M. Huang, C.-H. Hsu, I. Belopolski, N. Alidoust, D. S. Sanchez, H. Zheng, H. Lu, X. Zhang, Y. Bian, T.-R. Chang, H.-T. Jeng, A. Bansil, H. Hsu, S. Jia, T. Neupert, H. Lin *et al.*, Magnetic and noncentrosymmetric Weyl fermion semimetals in the *R*AlGe family of compounds (R = rare earth), Phys. Rev. B **97**, 041104(R) (2018).
[41] B. L. Gyorffy, Coherent-potential approximation for a nonoverlapping-muffin-tin-potential model of random substitutional alloys, Phys. Rev. B **5**, 2382 (1972).
[42] H. Ebert, D. Koedderitzsch, and J. Minar, Calculating condensed matter properties using the KKR-Green's function method—recent developments and applications, Rep. Prog. Phys. **74**, 096501 (2011).
[43] C. E. Patrick, G. A. Marchant, and J. B. Staunton, Spin orientation and magnetostriction of Tb_{1-x} Dy_xFe_2 from first principles, Phys. Rev. Appl. **14**, 014091 (2020).
[44] G. P. Müller, M. Hoffmann, C. Dißelkamp, D. Schürhoff, S. Mavros, M. Sallermann, N. S. Kiselev, H. Jónsson, and S. Blügel, *Spirit:* Multifunctional framework for atomistic spin simulations. Phys. Rev. B **99**, 224414 (2019).
[45] J. Bouaziz, H. Ishida, S. Lounis, and S. Blügel, Transverse transport in two-dimensional relativistic systems with nontrivial spin textures, Phys. Rev. Lett. **126**, 147203 (2021).
[46] J. P. Perdew and A. Zunger, Self-interaction correction to density-functional approximations for many-electron systems, Phys. Rev. B **23**, 5048 (1981).
[47] M. Lüders, A. Ernst, M. Däne, Z. Szotek, A. Svane, D. Ködderitzsch, W. Hergert, B. L. Györffy, and W. M. Temmerman, Self-interaction correction in multiple scattering theory, Phys. Rev. B **71**, 205109 (2005).
[48] P. Larson, W. R. L. Lambrecht, A. Chantis, and M. van Schilfgaarde, Electronic structure of rare-earth nitrides using the LSDA + U approach: Importance of allowing 4f orbitals to break the cubic crystal symmetry, Phys. Rev. B **75**, 045114 (2007).

[49] J.-F. Wang, Q.-X. Dong, Z.-P. Guo, M. Lv, Y.-F. Huang, J.-S. Xiang, Z.-A. Ren, Z.-J. Wang, P.-J. Sun, G. Li *et al.*, NdAlSi: A magnetic Weyl semimetal candidate with rich magnetic phases and atypical transport properties, Phys. Rev. B **105**, 144435 (2022).

[50] A. I. Liechtenstein, V. I. Anisimov, and J. Zaanen, Density-functional theory and strong interactions: Orbital ordering in Mott-Hubbard insulators, Phys. Rev. B **52**, R5467(R) (1995).

[51] E. Bousquet and N. Spaldin, J dependence in the LSDA + U treatment of noncollinear magnets, Phys. Rev. B **82**, 220402(R) (2010).

[52] S. L. Dudarev, G. A. Botton, S. Y. Savrasov, C. J. Humphreys, and A. P. Sutton, Electron-energy-loss spectra and the structural stability of nickel oxide: An LSDA + U study, Phys. Rev. B **57**, 1505 (1998).

[53] T. Wang, Y. Guo, and C. Wang, Structure and magnetic properties of RAlSi (R = light rare earth), Chin. Phys. B **30**, 075102 (2021).

[54] J. P. Perdew, K. Burke, and M. Ernzerhof, Generalized gradient approximation made simple, Phys. Rev. Lett. **77**, 3865 (1996).

[55] S. Pikus, E. Olszewska, I. Mel'nyk, and R. E. Gladyshevskii, X-ray powder diffraction analysis and initial Rietveld characterization of SmAlSi and SmAlGe, Powder Diffr. **19**, 359 (2004).

[56] A. Kokalj, XCrySDen – a new program for displaying crystalline structures and electron densities, J. Mol. Graphics Modell. **17**, 176 (1999).

[57] B. L. Gyorffy, A. J. Pindor, J. Staunton, G. M. Stocks, and H. Winter, A first-principles theory of ferromagnetic phase transitions in metals, J. Phys. F **15**, 1337 (1985).

[58] M. Richter, Band structure theory of magnetism in 3d-4f compounds, J. Phys. D **31**, 1017 (1998).

[59] J. Enkovaara, C. Rostgaard, J. J. Mortensen, J. Chen, M. Dułak, L. Ferrighi, J. Gavnholt, C. Glinsvad, V. Haikola, H. A. Hansen *et al.*, Electronic structure calculations with GPAW: a real-space implementation of the projector augmented-wave method, J. Phys.: Condens. Matter **22**, 253202 (2010).

[60] R. Skomski, *Simple Models of Magnetism* (Oxford University Press on Demand, Oxford, 2008).

[61] A. Szilva, Y. Kvashnin, E. A. Stepanov, L. Nordström, O. Eriksson, A. I. Lichtenstein, and M. I. Katsnelson, Quantitative theory of magnetic interactions in solids, Rev. Mod. Phys. **95**, 035004 (2023).

[62] S. Streib, A. Szilva, V. Borisov, M. Pereiro, A. Bergman, E. Sjöqvist, A. Delin, M. I. Katsnelson, O. Eriksson, and D. Thonig, Exchange constants for local spin Hamiltonians from tight-binding models, Phys. Rev. B **103**, 224413 (2021).